

# Characterisation of the secondary instability in a 1:3 sudden expansion through inviscid structural sensitivity

Roberta Santoriello, Flavio Giannetti , Franco Auteri and Vincenzo Citro

Corresponding author: Flavio Giannetti, fgiannetti@unisa.it

(Received 9 January 2025; revised 29 July 2025; accepted 5 October 2025)

The inviscid mechanism, driving flow instabilities in a 1:3, planar and symmetric sudden expansion, is discerned through a sensitivity-based protocol, also referred to as inviscid structural sensitivity analysis, with a specific focus on the onset and nature of the secondary instability. The fundamental idea of this methodology is to change the contribution of viscosity solely in the global stability equations, while freezing the baseflow field at the critical conditions. This is practically implemented by decoupling the Reynolds number that serves as the control parameter for determining the steady base flow from that governing the disturbance evolution, in order to repeat the structural sensitivity analysis while progressively increasing the Reynolds number in the linearised equations only. Accordingly, the sequence of structural sensitivity maps enables us to highlight the flow regions where the inviscid instability mechanism acts. The numerical results reveal that the classical structural sensitivity analysis accurately locates the wavemaker region within the primary recirculation zone, but only its inviscid limit can unveil that the core of the instability coincides with the centre of the primary vortex: a hallmark of an elliptic instability. To validate the global findings, the results of the inviscid structural sensitivity analysis are compared with those obtained from geometric optics. The agreement of the two approaches confirms the inviscid character of the instability, thereby providing a complete picture of the nature of the secondary bifurcation.

**Key words:** absolute/convective instability, bifurcation, separated flows

<sup>&</sup>lt;sup>1</sup>DIIN, University of Salerno, Via Giovanni Paolo II, 84084 Fisciano (SA), Italy

<sup>&</sup>lt;sup>2</sup>Dipartimento di Scienze e Tecnologie Aerospaziali, Politecnico di Milano, via La Masa 34, 20156 Milano, Italy

## 1. Introduction

Coherent structures play an undeniable role in many turbulent flows (Fiedler 1987). Identifying the critical conditions and the kind of instability that lead to the breakdown of these eddies is essential to grasp the behaviour and the organisation of fluid flows.

An interesting example is the flow in a symmetric planar sudden expansion, a classical configuration characterised by a symmetry-breaking bifurcation, whose first instability has been extensively investigated in previous studies. Experimental observations, carried out by several researchers, including Durst *et al.* (1974), Cherdron, Durst & Whitelaw (1978), Sobey & Drazin (1986), Fearn, Mullin & Cliffe (1990) and Durst *et al.* (1993) showed that, for moderate expansion ratios (i.e. outlet to inlet section), the primary flow is steady, two-dimensional and exhibits reflectional symmetry about the mid-plane of the channel, with two recirculation regions of equal size, past the steps of the expansion, that increase linearly with the Reynolds number. Above the instability threshold, the flow loses its symmetry via a pitchfork bifurcation and a pair of stable, steady and two-dimensional asymmetric flow states (secondary flow) evolve gradually, as one recirculation region grows at the expense of the other.

Subsequent numerical studies of this problem gave more insights into the flow-field organisation. For instance, Battaglia *et al.* (1997) identified the onset of the first bifurcation over a wide range of channel expansion ratios, showing that the critical Reynolds number decreases with higher expansion ratios, while Fani, Camarri & Salvetti (2012) investigated the stability properties of the flow in the context of the linear theory and performed a sensitivity analysis with respect to perturbations that may be produced by a realistic passive control, thus providing qualitative hints and quantitative pieces of information to design a control.

As the Reynolds number is increased further, the flow becomes time-dependent. Experimental observations from Sobey & Drazin (1986) demonstrated the evidence of a further pitchfork bifurcation, with symmetry breaking in the spanwise direction and thence the onset of a strongly three-dimensional flow (see figure 12 of Sobey & Drazin 1986). Also the investigations conducted by Fearn *et al.* (1990) and the numerical analysis performed by Battaglia *et al.* (1997) indicated that the flow becomes three-dimensional prior to becoming unsteady.

To delve deeper into the nature of this secondary instability, Lanzerstorfer & Kuhlmann (2012a) used an energy approach, as discussed later on. In particular, by varying the expansion ratio in a quasi-continuous way, they show that the asymmetric two-dimensional secondary flow becomes unstable to three-dimensional perturbations. For large expansion ratios, the critical mode passes from stationary to oscillatory and pure centrifugal and elliptical amplification processes are identified. However, in the case of moderate expansion ratios, e.g. 1:3 symmetric sudden expansion (which is the case of the present study where a stationary three-dimensional bifurcation is detected), the physical interpretation becomes challenging, since all the integral energy production rates are positive, making it difficult to attribute the instability to a single energy transfer process, therefore preventing them from assessing the character of the instability. Specifically, the combined effects of flow deceleration near the reattachment point, shear-induced amplification on both edges of the plane jet and streamline convergence in the downstream region of the separated flow, are generically indicated as the possible origins of the destabilisation.

In this context, the goal of the present work is to characterise the mechanism driving the global instability in the 1:3 sudden expansion, with the focus on the onset and nature

of the secondary instability, whose features are not yet understood. In particular, we show that the instability is elliptical, a particular kind of inviscid instability.

The concept of inviscid instability can be found in classical textbooks (Charru 2011) and it has been largely used to explain fluid instabilities in different flow configurations. According to Charru (2011), an inviscid instability '[...] owes its origin to the inertia of the fluids; [...] viscosity only attenuates the instability via diffusion, and plays a smaller role the higher the Reynolds number'. The elliptic, hyperbolic and centrifugal types of instability are notably characterised by inviscid mechanisms. In particular, the elliptical instability is a mechanism by which three-dimensional flows can be generated in regions of two-dimensional, elliptical streamlines. This mechanism is caused by resonance due to strain at elliptic stagnation points. Laboratory experiments (Leweke & Williamson 1998) and numerical modelling indicate the severity of the instability mechanism in that the flow quickly becomes complicated, typically leading to a breakdown to small-scale disorder. Theoretical investigations of the elliptical instability have been conducted by Bayly (1986), Pierrehumbert (1986), Landman & Saffman (1987) and Waleffe (1990), among others. For a comprehensive overview, the reader is referred to Kerswell (2002). The hyperbolic instability is due to stretching near hyperbolic stagnation points (see e.g. Friedlander & Vishik 1991; Leblanc 1997; Pralits, Giannetti & Brandt 2013), and it occurs on streamlines that pass through regions in the neighbourhood of hyperbolic points. The essential mechanism of the centrifugal instability was given by Rayleigh (1917), who introduced a criterion to ascertain instability in the inviscid case. This inviscid mechanism is due to the disruption of the balance between the centrifugal force and the radial pressure gradient and gives rise to modes which are localised along particular streamlines, with a transverse spatial structure which generally decays exponentially fast.

An appealing technique to study elliptic, hyperbolic and centrifugal instabilities is offered by the geometric optics (or short-wave asymptotics) stability approach that provides a robust framework for establishing local instability criteria (Lifschitz & Hameiri 1991). This method is based on the classical Wentzel–Kramers–Brillouin (WKB) approximation and has been successfully applied in the past to study inviscid instabilities developing on two-dimensional stationary base flows (see e.g. Lebovitz & Lifschitz 1996; Leblanc & Cambon 1997), in the short-wave limit. *Ad hoc* correction terms, accounting for finite wavenumbers and viscous damping (Landman & Saffman 1987), have been used by Gallaire, Marquillie & Ehrenstein (2007) with the aim of characterising the primary three-dimensional bifurcation of the flow past a bump.

The link between geometric optics and global stability analysis (Theofilis 2011) was first explored by Bayly (1988) in the case of centrifugal instabilities. He demonstrated how the short-wave asymptotic formalism could be used to construct localised amplified normal modes. Direct comparisons between linearised direct numerical simulation findings and short-wave asymptotic results (Bayly 1989) have also shown a qualitative agreement between the two techniques. Further assessment was given by Sipp & Jacquin (1998), who introduced a more quantitative approach to link the short-wave asymptotic and the normal mode analysis. They identify elliptical and centrifugal-type normal modes whose characteristics (spatial structures and eigenvalues) are in accordance with the results given by the geometrical optics method. Sipp, Lauga & Jacquin (1999) showed that different instability mechanisms are characterised by spatial support in different regions of the flow domain. By analysing a periodic array of two-dimensional flattened Taylor-Green vortices in a rotating frame, they illustrated that centrifugal eigenmodes are localised in the vicinity of closed streamlines in the anticyclones while elliptical eigenmodes are concentrated in the centre of the cyclones or anticyclones and hyperbolic eigenmodes are located near closed streamlines in cyclones. Godeferd, Cambon & Leblanc (2001) confirmed Sipp's prediction of short-wave instabilities by studying a street of Stuart vortices with external rotation.

Pinpointing inviscid mechanisms in real flow configurations proves to be challenging, prompting the application of multiple methodologies to capture the physical nature of the instabilities. Lanzerstorfer & Kuhlmann (2012a, 2012b, 2012c) proposed an *a posteriori* energy transfer method to reveal the character of the instabilities developing in plane-channel flows with geometric discontinuities, i.e. exhibiting sudden expansions/constrictions in the form of steps. However, as will be pointed out later, this approach is not always effective, as in some configurations, it fails to discern the underlying instability mechanism.

Given the lack of a robust methodology, it seems essential to adopt a reliable protocol to accurately detect the non-viscous nature of the amplification process. In the present paper, we rely on structural sensitivity analysis to identify the inviscid core that triggers the feedback mechanism responsible for the instability. The key ingredient of this sensitivitybased protocol, also referred to as inviscid structural sensitivity analysis, lies in making viscosity effects vanish solely in the global stability equations while maintaining the baseflow field constant, computed at the critical Reynolds number. As a matter of fact, the idea of decoupling the Reynolds number in the base flow and in the perturbation dynamics is not new, it has been common practice since the work of Lord Rayleigh (1879). When the instability mechanism is inviscid, removing viscosity from the linear stability analysis allows us to remove diffusion phenomena from the model, keeping just the inviscid phenomena that are responsible for the instability. Clearly, the effects of viscosity must be taken into account to have an accurate, quantitative description of the instability, but, when an inviscid instability mechanism is at play, computing the inviscid structural sensitivity is of help to locate and identify the instability mechanism. An important aspect related to assessing and locating the inviscid instability mechanism is that, once the inviscid nature and type of the instability (i.e. elliptic, hyperbolic or centrifugal) are characterised, a connection between global and local analyses can be established. This allows for the reconstruction of global modes from local approaches, providing a more comprehensive understanding of the instability behaviour (Bayly 1988; Sipp & Jacquin 1998). Indeed, the local approach provides a robust framework for gaining deeper physical insight into the underlying instability, and it is more efficient than global stability analysis from a computational perspective, as it involves the simple integration of a tiny set of ordinary differential equations in one dimension.

Citro et al. (2015) used the inviscid structural sensitivity analysis to study the incompressible flow past a square open cavity. The authors attributed the nature of the instability to a centrifugal mechanism due to the localisation of the inviscid sensitivity field around a critical orbit, that was the same as that identified by the short-wave asymptotic analysis. More recently, Chiarini & Auteri (2023) employed this method to assess the inviscid character of the primary (regular) bifurcation of the steady, twodimensional flow past rectangular cylinders moving along a wall. For small gap heights and elongated cylinders, they found that the inviscid structural sensitivity analysis closely aligns with the results predicted from geometric optics, putting forward some evidence that the centrifugal instability plays a role in the triggering mechanism. Thus, as the local analysis is able to accurately predict the particle orbit that provides the main contribution to the instability, the inviscid structural sensitivity can sharply localise the key features of the bifurcation on closed trajectories or critical points. More specifically, in agreement with the aforementioned framework proposed by Sipp et al. (1999), in the case of an elliptical instability, the maximum value of the inviscid structural sensitivity is expected at the centre of an elliptical vortex, while, for the hyperbolic and centrifugal mechanisms,

higher sensitivity values are found along streamlines near hyperbolic stagnation points and along closed streamlines within the recirculating regions, respectively. In this context, the sensitivity protocol acts as a magnifying glass, capable of clearly isolating the location of the inviscid core, thereby completing the picture provided by Lanzerstorfer and Kuhlmann. To the authors' knowledge, we present the first agreement between an asymptotic WKB expansion and global stability results for an elliptic instability.

The paper is organised as follows. The second section ( $\S 2$ ) is devoted to the description of the geometrical configuration of the problem and its mathematical formulation, while § 3 concerns the global linear stability analysis, providing an accurate estimation of the secondary bifurcation instability threshold (the critical Reynolds number and the corresponding spanwise wavenumber are determined). Then, in § 4, the adjoint-based structural sensitivity analysis is performed to localise the region in the flow with the role of wavemaker in the excitation of the global instability. Section 5 is the heart of the paper since it deals with the inviscid structural sensitivity analysis that allows us to unveil the physical nature of the instability. Successively, in § 6, we pursue the study by investigating the mechanism of instability through the geometric optics method, to validate the predictions provided by the sensitivity protocol. Each section is organised to first present the fundamental theory behind the methodology employed, followed by a discussion of the related results. This structure is intended to clarify the specific contribution provided by each analysis (that is also recalled in the section titles). Finally, a synthesis of the results and concluding remarks are given in § 7. In the appendices, we provide a brief description of the numerical methods employed for the global linear stability analysis (Appendix A) and the short-wave asymptotic (Appendix B).

# 2. The flow in a plane symmetric sudden expansion

#### 2.1. Geometrical configuration

The analysis presented here concerns the flow of a Newtonian fluid through a symmetric sudden expansion. With reference to figure 1, the flow is coming from the left at the inlet of a channel of height d and length  $L_{in} = 5d$ , followed by a sudden enlargement in a planar duct of height D = 3d, whose length  $L_{out} = 50d$  has been chosen to recover a plane Poiseuille flow at the downstream end of the channel. Let ER = D/d be the ratio of the height of the channel downstream (D) and upstream (d) the geometrical discontinuity. In this study, a value of the expansion ratio ER = 3 has been considered (as, for instance, in Fearn et al. 1990; Hawa & Rusak 2000; Fani et al. 2012, among others).

The origin of the Cartesian reference frame is placed at the midpoint of the inlet edge  $(\partial \mathcal{D}_{in})$ , denoting the streamwise, wall-normal and spanwise directions with x, y and z, respectively. The base flow is assumed to be two-dimensional and homogeneous in the spanwise direction (z).

The separation and reattachment points of the three recirculation regions (that characterise the secondary asymmetric flow field) are also qualitatively represented in figure 1.

#### 2.2. Problem statement

The fluid motion is governed by the unsteady incompressible Navier-Stokes equations that, in non-dimensional form, can be written as follows:

$$\frac{\partial \mathbf{u}}{\partial t} + (\mathbf{u} \cdot \nabla) \mathbf{u} = -\nabla P + \frac{1}{Re} \nabla^2 \mathbf{u}, \qquad (2.1a)$$

$$\nabla \cdot \mathbf{u} = 0, \qquad (2.1b)$$

$$\nabla \cdot \boldsymbol{u} = 0. \tag{2.1b}$$

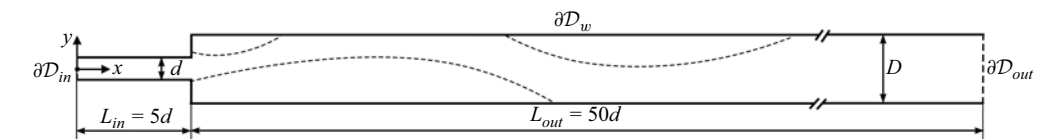


Figure 1. Symmetric sudden expansion geometry. Dashed lines qualitatively represent the recirculation regions.

where u is the velocity vector,  $u(x, t) = (u, v, w)^T$ , P(x, t) is the reduced pressure field and  $x = (x, y, z)^T$  indicates the spatial coordinates, while t denotes time.

Equations (2.1) are made dimensionless using the height of the channel before the expansion (d) and the maximum (centreline) velocity  $(U_c)$  of the incoming flow as reference scales for the length and for the velocity, respectively. The Reynolds number (Re) is thus defined as

$$Re = \frac{U_c d}{v},\tag{2.2}$$

with  $\nu$  the fluid kinematic viscosity.

The boundary conditions complete the system of differential equations, (2.1): at the inlet  $(\partial \mathcal{D}_{in})$ , a fully developed Poiseuille velocity profile is prescribed, no-slip boundary conditions are imposed along the solid walls of the channel  $(\partial \mathcal{D}_w)$ , while a traction-free condition is enforced at the outlet  $(\partial \mathcal{D}_{out})$  of the domain

$$\begin{cases}
\mathbf{u} = U_c \left( 1 - \left( \frac{2y}{d} \right)^2 \right) \mathbf{e}_x, & \forall \mathbf{x} \in \partial \mathcal{D}_{in} \text{ (inlet),} \\
\mathbf{u} = \mathbf{0}, & \forall \mathbf{x} \in \partial \mathcal{D}_w \text{ (wall),} \\
P\mathbf{n} - Re^{-1} (\nabla \mathbf{u} \cdot \mathbf{n}) = \mathbf{0}, & \forall \mathbf{x} \in \partial \mathcal{D}_{out} \text{ (outlet),}
\end{cases}$$
(2.3)

where  $e_x$  is the unit vector in the direction of the x-axis, while n denotes the surface-normal vector (in this case, it is the vector perpendicular to the outlet of the computational domain).

# 3. Global linear stability analysis: the threshold of the secondary instability

## 3.1. Methodology

## 3.1.1. Base flow and direct eigenvalue problem

The onset of the secondary instability is investigated by a classical linear stability analysis (LSA). Thus, the total flow field  $\mathbf{Q} = (\mathbf{u}, P)^T$  is assumed as the sum of a steady, two-dimensional base flow (or basic state)  $\mathbf{Q}_b$  and a time-dependent, three-dimensional perturbation  $\mathbf{q}'$ , i.e. a small deviation from the base flow of amplitude  $\epsilon$ , so that

$$Q(x,t) = \begin{pmatrix} u \\ P \end{pmatrix}(x,t) = Q_b(x) + \epsilon q'(x,t), \tag{3.1}$$

where

$$\mathbf{Q}_b(x, y) = (\mathbf{u}_b, P_b)^T = (u_b, v_b, 0, P_b)^T, \tag{3.2a}$$

$$\mathbf{q}'(x, y, z, t) = (\mathbf{u}', P')^{T} = (u', v', w', P')^{T}.$$
 (3.2b)

Substituting the decomposition (3.1) into the system of differential equations, (2.1), and neglecting quadratic terms, two systems can be obtained that describe the spatial structure of the base flow and the evolution of perturbations.

The base flow is solution of the steady version of (2.1)

$$\begin{cases} (\boldsymbol{u}_b \cdot \nabla) \, \boldsymbol{u}_b = -\nabla P + \frac{1}{Re_{BF}} \nabla^2 \boldsymbol{u}_b, \\ \nabla \cdot \boldsymbol{u}_b = 0, \end{cases}$$
(3.3)

supplemented with the boundary conditions listed in (2.3), while the perturbed field is governed by the linearised, unsteady Navier–Stokes equations (LNSEs)

$$\begin{cases}
\frac{\partial \mathbf{u}'}{\partial t} + \mathbf{L} \{\mathbf{u}_b(Re_{BF}), Re_{STB}\} \mathbf{u}' + \nabla P' = \mathbf{0}, \\
\nabla \cdot \mathbf{u}' = 0,
\end{cases}$$
(3.4)

where L stands for the linearised Navier–Stokes operator that in vector notation can be written as follows:

$$L\{u_b(Re_{BF}), Re_{STB}\} u' = u_b \cdot \nabla u' + u' \cdot \nabla u_b - \frac{1}{Re_{STB}} \nabla^2 u'.$$
 (3.5)

In the above systems (3.3–3.4), the Reynolds number (defined as in 2.2) used for base-flow computations (3.3) is denoted as  $Re_{BF}$ , while the Reynolds number used in the LNSEs (3.4) is labelled as  $Re_{STB}$ . This notation is intended to decouple the Reynolds number that serves as the control parameter for determining the steady base flow, from the Reynolds number that governs the evolution of perturbations (as required by the inviscid structural sensitivity framework discussed in § 5). Henceforth, when  $Re_{BF} = Re_{STB}$  we simply use Re.

Exploiting the homogeneity of the base flow in the spanwise direction (z), the perturbation (q') can be expressed using the normal mode decomposition as

$$q'(x, y, z, t) = \hat{q}(x, y)e^{\gamma t + ikz} + \text{c.c.},$$
 (3.6)

where the term c.c. stands for complex conjugate, while  $\hat{q} = (\hat{u}, \hat{P})^T = (\hat{u}, \hat{v}, \hat{w}, \hat{P})^T$  denotes the global (direct) eigenfunction and  $\gamma = \sigma + i\omega$  is the complex eigenvalue, that comprises the real growth/decay rate of the perturbation  $(\sigma)$  and its oscillation circular frequency  $(\omega)$ . Together, eigenvectors and eigenvalues are called the eigenmodes or global modes.

Injecting the modal ansatz (3.6) into the LNSEs (3.4), the following two-dimensional (so-called biglobal) generalised (direct) eigenvalue problem (EVP) is obtained:

Direct EVP: 
$$\begin{cases} \gamma \ \hat{\boldsymbol{u}} + \boldsymbol{L} \{ \boldsymbol{u}_b(Re_{BF}), Re_{STB} \} \ \hat{\boldsymbol{u}} + \nabla \hat{P} = \boldsymbol{0}, \\ \nabla \cdot \hat{\boldsymbol{u}} = 0. \end{cases}$$
(3.7)

For a given k, the complex  $\gamma$  can be computed by solving the stability problem (3.7), complemented with the following boundary conditions:

$$\begin{cases}
\hat{\boldsymbol{u}} = \boldsymbol{0}, & \text{on } \partial \mathcal{D}_{in} \cup \partial \mathcal{D}_{w} \text{ (inlet and wall),} \\
\hat{P}\boldsymbol{n} - Re_{STB}^{-1}(\nabla \hat{\boldsymbol{u}} \cdot \boldsymbol{n}) = \boldsymbol{0}, & \text{on } \partial \mathcal{D}_{out} \text{ (outlet).}
\end{cases}$$
(3.8)

If all the eigenvalues  $(\gamma)$  are such that  $\sigma$  is negative, then the base flow is stable with respect to small three-dimensional perturbations (i.e. the disturbance is damped). If, on the other hand, there exists at least one eigenvalue with positive real part, then the base flow is unstable (i.e. the disturbance is amplified), namely the perturbations (q') grow with time and the flow will evolve away from its initial state  $(Q_h)$ .

# 3.1.2. Adjoint eigenvalue problem

To determine the instability core by means of the adjoint-based structural sensitivity analysis (in § 4), the study of both the direct and adjoint modes is required. In particular, the adjoint global mode represents the receptivity of the direct mode to external forcing.

Following the framework introduced by Giannetti & Luchini (2007), the adjoint perturbation  $\hat{q}^{\dagger} = (\hat{u}^{\dagger}, \hat{P}^{\dagger})^T$  satisfies the following equations:

Adjoint EVP: 
$$\begin{cases} -\gamma \hat{\boldsymbol{u}}^{\dagger} + \boldsymbol{L}^{\dagger} \{\boldsymbol{u}_{b}(Re_{BF}), Re_{STB}\} \hat{\boldsymbol{u}}^{\dagger} + \nabla \hat{P}^{\dagger} = \boldsymbol{0}, \\ \nabla \cdot \hat{\boldsymbol{u}}^{\dagger} = 0. \end{cases}$$
(3.9)

with corresponding boundary conditions and  $L^\dagger$  the adjoint linearised Navier–Stokes operator expressed as

$$L^{\dagger}\{u_b(Re_{BF}), Re_{STB}\}u'^{\dagger} = u_b \cdot \nabla u'^{\dagger} - \nabla u_b \cdot u'^{\dagger} + \frac{1}{Re_{STB}} \nabla^2 u'^{\dagger}. \tag{3.10}$$

More details on the derivation of the adjoint problem can be found in Giannetti & Luchini (2007), while for a complete review of the role of the adjoint equations in stability analysis the reader is referred to Luchini & Bottaro (2014).

## 3.2. Results

As is well known from the literature (Fani *et al.* 2012), the flow in a 1:3 plane sudden expansion remains symmetric for Reynolds numbers below  $Re_{cr}^{(I)} \approx 81$ . However, under supercritical conditions, while the flow remains two-dimensional and steady, it becomes asymmetric.

We perform a global LSA around this secondary flow to investigate the onset of the secondary bifurcation. The numerical results, shown in figure 2, reveal that the flow undergoes a steady ( $\omega=0$ ; see figure 2b), three-dimensional ( $k\neq 0$ ) bifurcation at a critical Reynolds number of approximately  $Re_{cr}^{(II)}\approx 306$ , associated with spanwise wavenumber  $k\approx 0.65$  (figure 2a), in agreement with previous numerical investigations (see e.g. Lanzerstorfer & Kuhlmann 2012a). The eigenvalue spectrum (at  $Re_{cr}^{(II)}=306$  and k=0.65), illustrated in figure 3, shows that the eigenvalues are real or come in complex-conjugate pairs, as expected, and that the least stable eigenvalues are discrete.

The structure of the base flow, computed at the critical Reynolds number, is depicted in figure 4. The flow separates from the lower wall, impinges on the upper edge of the domain and then reattaches to the bottom wall. This phenomenon is usually explained by a Coanda effect, that is a consequence of the pressure difference established in the cross-stream direction (see the early work by Bourque & Newman 1960). The resulting asymmetric flow field can have one of two specular orientations, corresponding to the main stream being diverted towards one wall of the channel or the other. In particular, there is

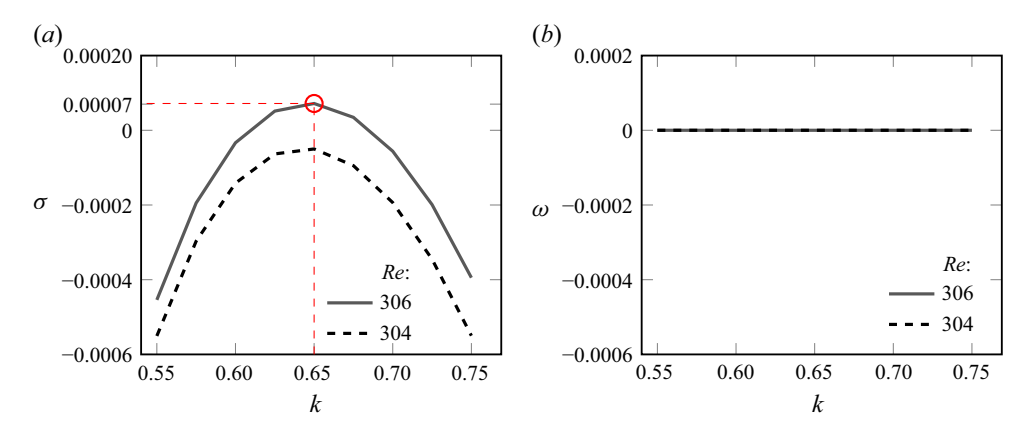


Figure 2. (a) Growth rate  $\sigma$  and (b) frequency  $\omega$  of the least-damped eigenvalue  $\gamma$  as a function of the spanwise wavenumber k, for the cases: Re = 304 (dashed line) and the critical value  $Re = Re_{cr}^{(II)} = 306$  (solid line). The red marker in (a) highlights the value of the wavenumber (k = 0.65) corresponding to the maximum amplification rate for the case Re = 306.

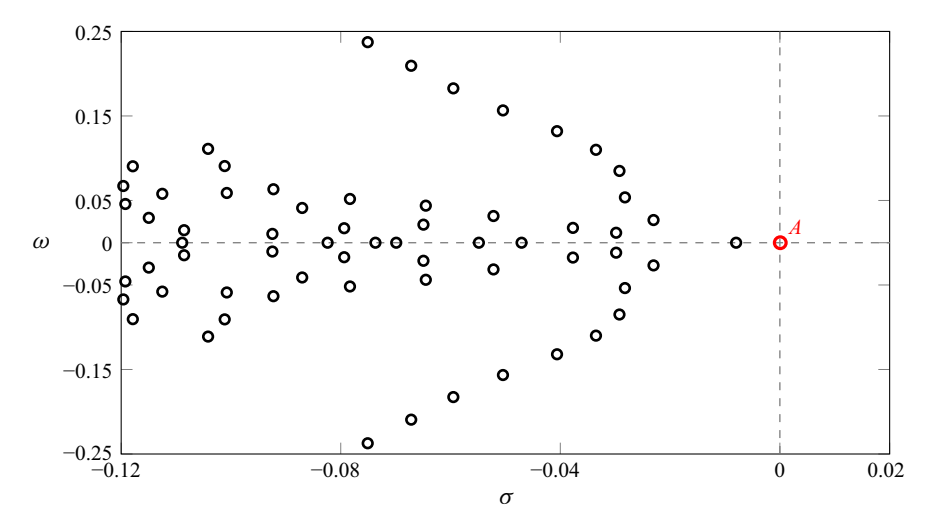


Figure 3. Eigenvalue spectrum at  $Re = Re_c^{(II)} = 306$  and k = 0.65. The red marker, labelled with the letter A, indicates the least stable eigenvalue, with coordinates  $(7 \times 10^{-5}, 0)$  in the plane  $(\sigma, \omega)$ .

an equal probability of the jet bending towards the upper or the lower side of the domain. The streamline plot, of one of the two possible asymmetric flows, shows that the flow field is characterised by three recirculation bubbles. Two of them separate immediately past the sharp corners, with the larger vortex referred to as the primary vortex, while the smaller one, on the opposite side of the channel, is denoted as the secondary vortex. Further downstream, on the same side of the secondary vortex, a third separated region arises (tertiary vortex), while at a streamwise distance of approximately x = 35, the flow recovers its parabolic profile.

The features of the bifurcation can be described by investigating the spatial structure of the direct and adjoint global eigenfunctions, computed at the critical conditions (figure 5). The absolute value of the fluctuating velocity field and its adjoint are depicted in figure 5(a,e). It can be observed that the direct mode (figure 5a) is strictly confined

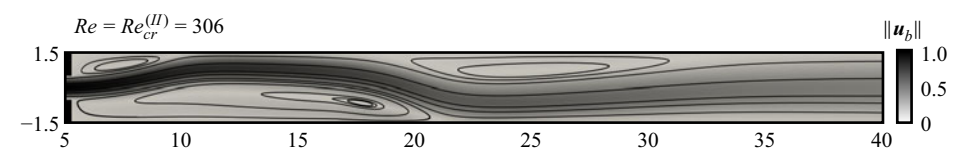


Figure 4. Stationary, two-dimensional and asymmetric base flow computed at the critical Reynolds number  $(Re = Re_{cr}^{(II)} = 306)$ . The contour plot displays the modulus of the velocity field, while solid lines indicate the streamlines inside the domain.

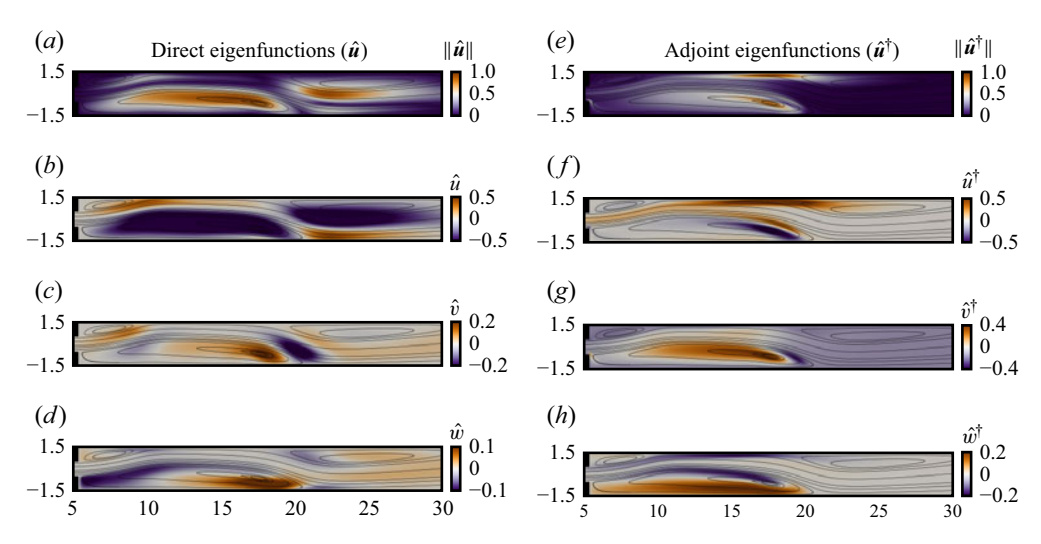


Figure 5. Spatial structure of the direct and adjoint eigenfunctions at the critical Reynolds number ( $Re = Re_{cr}^{(II)} = 306$ ) associated with a spanwise wavenumber k = 0.65: (a) modulus, (b) streamwise  $\hat{u}$ , (c) cross-stream  $\hat{v}$  and (d) spanwise  $\hat{w}$  velocity (direct) perturbed components. Similarly, (e-h) depict the corresponding adjoint eigenfunctions.

within the primary recirculation region and around the tertiary vortex, while for the adjoint mode (figure 5e) the main contribution of the perturbation is localised close to the primary vortex core, on the upper wall of the domain, and it decays moving toward the outlet of the channel.

With reference to the direct eigenfunctions (figure 5b-d), the *u*-perturbation is the strongest, with the cross-stream ( $\hat{v}$ ) and spanwise ones ( $\hat{w}$ ) being respectively approximately 29.7% and 17.3% of the streamwise fluctuations. On the other hand, the adjoint field (figure 5f-h) reveals that the maximum receptivity is reached near the upper edge of the domain and the downstream side of the primary vortex for the streamwise velocity component ( $\hat{u}^{\dagger}$ ), whereas in the cross-stream ( $\hat{v}^{\dagger}$ ) and spanwise ( $\hat{w}^{\dagger}$ ) directions, the fluctuations are most evident inside the primary recirculation region and the bottom wall, respectively (in particular,  $\hat{v}^{\dagger} \approx 0.524 \ \hat{u}^{\dagger}$  and  $\hat{w}^{\dagger} \approx 0.241 \ \hat{u}^{\dagger}$ ).

## 4. Structural sensitivity analysis: the core of the instability

## 4.1. *Methodology*

To investigate the physical mechanism responsible for the instability, we compute the structural sensitivity, which allows us to localise the core of the global instability, i.e. the 'active' flow regions where the amplification of the perturbations and receptivity

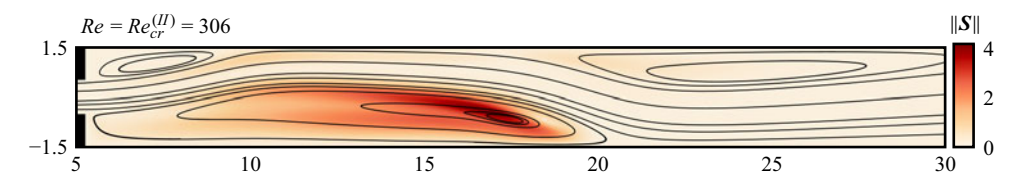


Figure 6. Structural sensitivity map, showing the core of the instability at the critical conditions  $(Re = Re_{CP}^{(II)} = 306, k = 0.65).$ 

combine to trigger the instability. The fundamental idea of such approach was introduced by Giannetti & Luchini (2007) in an attempt to extend to strongly non-parallel flows the concept of 'wavemaker', first introduced in the asymptotic analysis of slowly evolving flows by Huerre & Monkewitz (1990). Thus, following Giannetti & Luchini (2007), the structural sensitivity tensor can be evaluated by combining the direct  $(\hat{\boldsymbol{u}})$  and adjoint  $(\hat{\boldsymbol{u}}^{\dagger})$  eigenvectors

$$S(x_0, y_0; Re) = \frac{\hat{\boldsymbol{u}}^{\dagger} \, \hat{\boldsymbol{u}}}{\int_{\mathcal{D}} \hat{\boldsymbol{u}}^{\dagger} \cdot \hat{\boldsymbol{u}} \, dV}.$$
 (4.1)

The tensor S gives the shift in the eigenvalue produced by a velocity feedback localised at  $(x_0, y_0)$ . Here,  $\hat{u}^{\dagger}$   $\hat{u}$  stands for the dyadic product of the two vectors.

A spatial sensitivity map is then traced by computing the norm of the tensor at each point of the domain (see Giannetti & Luchini 2007 for details). Large values of S identify the regions where the localised feedback produces the largest drift in the growth rate or in the frequency of the mode. As in Giannetti & Luchini (2007), here, we use the Frobenius norm of this sensitivity tensor to identify where a modification in the linearised equations produces the greatest drift of the eigenvalue and thereby reveal the region of the flow that acts as the wavemaker.

#### 4.2. Results

The spatial distribution of the sensitivity tensor, computed at the critical Reynolds number, is depicted in figure 6. It can be observed that the primary recirculation bubble is the most sensitive region of the flow, as the structural sensitivity field is highly localised therein and its peak spreads near the primary vortex centre. Additional information could be gained by inspecting the absolute value of the individual components of the sensitivity tensor (as proposed by Qadri et al. 2013, 2015). This analysis allows us to distinguish the direct and adjoint velocity components that take a relevant role in the feedback process. All the components depicted in figure 7 show spatial support within the primary recirculation bubble. It is evident that the spatial structure of the sensitivity tensor is essentially due to the three components related to the streamwise velocity of the direct global mode (figure 7a,b,c). Thus, we can state that the feedback process consists of a loop in which the streamwise perturbations couple with the local receptivity of the flow in all the spatial directions. Although this analysis allows us to visualise the flow regions where feedback between the components of the velocity is strong, one can hardly assess the character of the instability simply based on the inspection of these maps. In particular, it is not clear whether the wavemaker is linked to the vortex centre (see e.g. figure 7a,b) or whether the core of the instability is distributed over a closed streamline (see e.g. figure 7c), that plays a crucial role in the feedback process. The question of the nature of the amplification process, operating within the primary recirculation zone, is addressed in the next section ( $\S 5$ ).

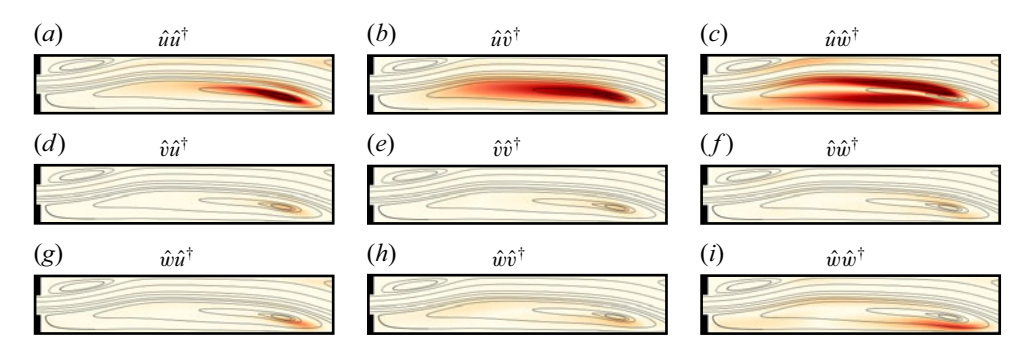


Figure 7. The absolute values of the components of the sensitivity tensor S at the critical Reynolds number  $(Re = Re_{cr}^{(II)} = 306)$  associated with a spanwise wavenumber k = 0.65. The shading on all the plots is scaled from 0 (white) to 2 (red). Each frame spans 0 < x < 20 on the horizontal axis and -1.5 < y < 1.5 on the vertical axis.

# Inviscid structural sensitivity: the identification of the instability physical mechanism

# 5.1. *Methodology*

The sensitivity analysis performed in the previous section (§ 4) clearly shows that the core of the three-dimensional instability, leading to the secondary bifurcation, is confined within the primary recirculation bubble. However, this observation is insufficient to unveil the underlying physical process, even if the relatively compact spatial support of the structural sensitivity field, whose peak spreads near the primary vortex centre, and the presence of locally closed elliptical streamlines in the core vortex, suggest that the instability could be associated with an inviscid mechanism.

Sipp *et al.* (1999) showed that different inviscid instabilities are characterised by spatial supports in different regions of the flow domain. Specifically, centrifugal and elliptic eigenmodes are concentrated along closed streamlines and in the vortex centres, respectively. However, a simple inspection of the sensitivity map (see figure 6) does not clarify whether the wavemaker is linked to the vortex centre or whether the core of the instability is distributed over a closed streamline, that plays a crucial role in the feedback process.

To shed light on the physical nature of the secondary bifurcation, and to assess whether it is of centrifugal or elliptic type, we aim at isolating the effect of the inviscid mechanism through a sensitivity-based protocol. The fundamental idea is to decouple the system of equations that govern the base flow from those that describe the disturbance evolution (as anticipated in § 2 with the notation  $Re_{STB}$  and  $Re_{BF}$ ) to change the viscosity effects solely in the global stability equations, while maintaining the base-flow field constant.

From a practical standpoint, we freeze the base flow at the critical Reynolds number ( $Re_{BF} = Re_{cr}^{(II)} = 306$ ) and then repeat the structural sensitivity analysis while progressively increasing  $Re_{STB}$  in the linearised equations. The resulting inviscid structural sensitivity tensor is thereby a function of both the base flow ( $Re_{BF}$ ) and the stability ( $Re_{STB}$ ) Reynolds number

$$S^*(Re_{BF}, Re_{STB}) = \frac{\hat{\boldsymbol{u}}^{\dagger}(\boldsymbol{u}_b(Re_{BF}); Re_{STB}) \, \hat{\boldsymbol{u}}(\boldsymbol{u}_b(Re_{BF}); Re_{STB})}{\int_{\mathcal{D}} \hat{\boldsymbol{u}}^{\dagger} \cdot \hat{\boldsymbol{u}} \, dV}.$$
 (5.1)

The norm of  $S^*$  can then be used to trace the inviscid structural sensitivity map. If the latter concentrates in a specific spatial region as  $Re_{STB}$  goes to infinity, then one can conjecture

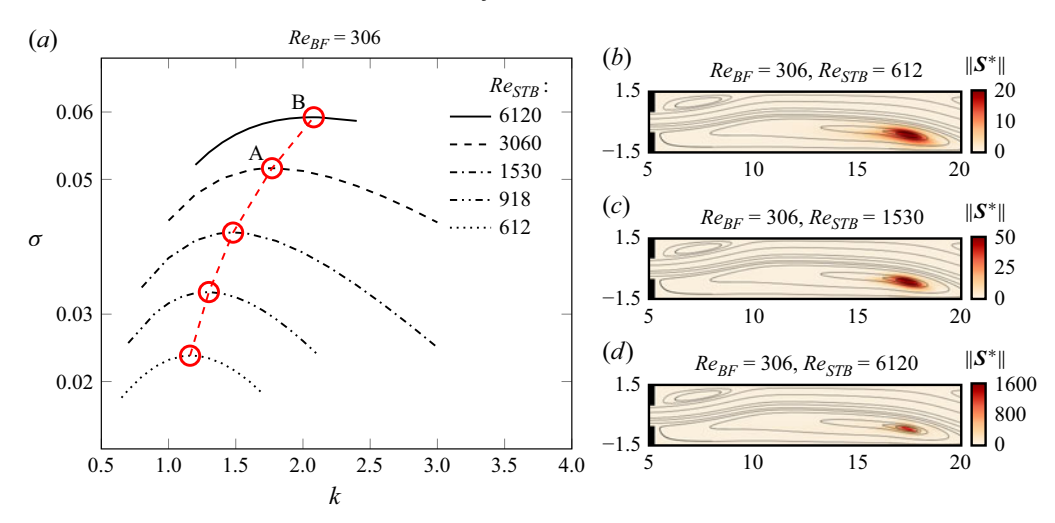


Figure 8. Inviscid structural sensitivity results at  $Re_{BF} = Re_{cr}^{(II)} = 306$ , while progressively increasing  $Re_{STB}$  in the LNSEs only. (a) Growth rate  $\sigma$  vs spanwise wavenumber k. The red markers denote the maximum of the curves. The last two points are labelled with the letters A and B as they will be referenced in the subsequent section (§ 6). (b-d) Inviscid structural sensitivity maps at (b)  $Re_{STB} = 612$ , (c)  $Re_{STB} = 1530$  and (d)  $Re_{STB} = 6120$ .

that an inviscid instability mechanism is at play and determine the flow regions where it acts.

#### 5.2. Results

The results given by the inviscid structural sensitivity analysis are plotted in figure 8(a). The graph shows the evolution of the growth rate  $(\sigma)$  associated with the unstable global mode under consideration as a function of the spanwise wavenumber (k) for several stability Reynolds numbers. In particular, numerical experiments were conducted at  $Re_{BF} = 306$  and  $Re_{STB} = 612, 918, 1530, 3060, 6120$ . It can be observed that, as ReSTB increases, the curves reach their peaks (highlighted by the red markers in the figure) at progressively higher wavenumbers (this aspect is discussed in detail in the following section § 6). By observing the spatial structure of the inviscid sensitivity tensor (figure 8b-d), it is evident that, as  $Re_{STR}$  becomes larger, the wavemaker tends to focus in the primary vortex centre. Furthermore, the spatial support of these fields is concentrated around their maximum values. These results preclude a centrifugal instability from being at play and suggest that the amplification process could be associated with an elliptic mechanism. In particular, by inspecting the spatial distribution of the structural sensitivity field, computed at the maximum  $Re_{STB}$  considered (equal to 6120) (figure 8d), it is evident that the critical mode is confined within the primary eddy and is strongest in its centre, which is a hallmark of an elliptic instability (see Bayly 1986; Pierrehumbert 1986; Waleffe 1990; Kerswell 2002, for a comprehensive description of the elliptic instability mechanism).

In summary, our findings indicate that the classical structural sensitivity (S) effectively identifies the wavemaker within the primary recirculation bubble (see figure 6 of § 4). However, it is only the inviscid structural sensitivity field ( $S^*$ ) that reveals that the instability core is concentrated around the centre of an elliptical vortex (see figure 8d).

Therefore, our results complete the picture proposed by Lanzerstorfer & Kuhlmann (2012a). Using an a posteriori energy transfer method, they observed that the flow dynamics changes with the expansion ratio. For large expansion ratios (i.e.  $3.484 \le ER \le 10$ ; note that this range has been redefined according to our definition of ER) the critical mode passes from stationary to oscillatory and pure centrifugal and elliptical amplification processes are identified. However, for moderate expansion ratios (1.538  $\le ER \le 3.334$ ), which is the case of the present study where a stationary three-dimensional bifurcation is detected, the physical interpretation becomes challenging and the energy approach fails to predict the inviscid character of the instability. The authors argue that, in the moderate expansion ratios range, the flow becomes unstable due to streamline convergence within the downstream side of the primary vortex, in combination with flow deceleration near the reattachment point, and an amplification process due to shear stresses near and between the primary and tertiary vortex. In contrast, by using inviscid structural sensitivity analysis, we demonstrate that an elliptic instability is already present in the steady regime.

In this context, the sensitivity protocol acts as a magnifying glass, allowing us to clearly isolate the inviscid core of the instability, thereby completing the characterisation of the secondary instability also for moderate *ERs*. Furthermore, the sensitivity protocol presented in this work is a general concept that can be used to discern any inviscid-type instability. Thus, this method can effectively be used also in other flow configurations (see for instance the works of Citro *et al.* 2015; Chiarini & Auteri 2023), to unveil the inviscid character of an instability, thereby enhancing the insight into the mechanism whereby complex three-dimensional motion can arise directly from two-dimensional coherent structures.

# 5.3. Results for a large expansion ratio

The geometric configuration examined in this study is known to exhibit different instability mechanisms depending on the value of the expansion ratio (Lanzerstorfer & Kuhlmann 2012a). Here, we demonstrate the effectiveness of the sensitivity-based protocol in detecting inviscid instabilities in a different configuration, specifically one characterised by ER = 20. As in Lanzerstorfer & Kuhlmann (2012a), we found that the flow undergoes an unsteady three-dimensional bifurcation at a critical Reynolds number of approximately  $Re_{cr}^{(II)} \approx 42.9$ , associated with a spanwise wavenumber of  $k \approx 0.13$  and an oscillation circular frequency of  $\omega \approx 0.048$ .

To assess the physical mechanism responsible for the instability, we compute both the classical and the inviscid structural sensitivity fields. The results are depicted in figure 9. It can be observed that, at the critical Reynolds number, the structural sensitivity field appears to be spatially diffused (figure 9a). However, by inspecting the inviscid sensitivity field computed at  $Re_{STB} = 100$  and  $Re_{STB} = 3000$  (figure 9b-c), it is evident that as  $Re_{STB}$  increases, the wavemaker tends to focus around a closed orbit, as expected for a centrifugal instability. Thus, in accordance with the energetic approach of Lanzerstorfer & Kuhlmann (2012a), it is possible to attribute the nature of the instability to a centrifugal mechanism due to the localisation of the inviscid sensitivity field around a closed streamline that falls in a region in which the Rayleigh (1917) criterion is valid (see figure 12 of Lanzerstorfer & Kuhlmann 2012a). In conclusion, we highlight that, not only is the inviscid structural sensitivity able to identify the centrifugal character of the instability associated with a closed streamline in the recirculating region, but it also accurately predicts the particle orbit that provides the main contribution to the instability.

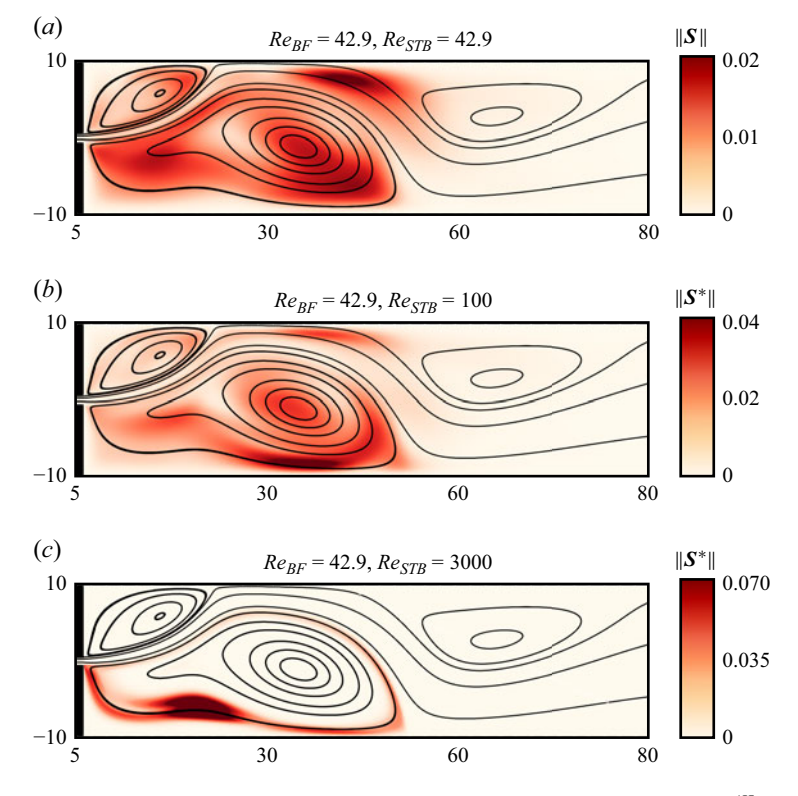


Figure 9. Inviscid structural sensitivity results for the case ER = 20, at  $Re_{BF} = Re_{cr}^{(II)} = 42.9$ , while progressively increasing  $Re_{STB}$  in the LNSEs only. Panels show (a)  $Re_{BF} = Re_{STB} = 42.9$ , (b)  $Re_{BF} = 42.9$  and  $Re_{STB} = 100$ , (c)  $Re_{BF} = 42.9$  and  $Re_{STB} = 3000$ , plotted at the optimal spanwise wavenumber.

# 6. The short-wave asymptotic stability analysis: the elliptic instability

## 6.1. Methodology

To confirm the evidence, given by the inviscid structural sensitivity analysis (in § 5) of an elliptical instability mechanism, we pursue the investigation using a local theory based on the geometric optics (or short-wave asymptotic) approach. This theory has been successfully applied in the past to study elliptic, hyperbolic and centrifugal instabilities developing on two-dimensional stationary base flows. It is based on the fact that short-wave instabilities can be described as localised wave envelops that move along trajectories of fluid elements. The motion is governed by a system of characteristic equations along the corresponding trajectories, consisting of the eikonal equation for the wavenumber and the transport equation for the velocity amplitude. Thus, the burden of proof that a given flow is unstable is placed on the analysis of ordinary differential equations along trajectories of fluid elements rather than of the three-dimensional Euler equations for perturbations (Lifschitz 1994). In the following, this approach is briefly presented; for a detailed description, the reader is referred to the work of Lifschitz & Hameiri (1991) in which the whole theory is thoroughly explained and applied.

Within the classical WKB approximation, the solution of the LNSEs (3.4) is sought in the form of a localised rapidly oscillating wave packet evolving along a closed Lagrangian trajectory, X(t) such that

$$\mathbf{u}'(X,t) = e^{i\frac{\phi(X,t)}{\epsilon}} \mathbf{a}(X,t,\epsilon) = e^{i\frac{\phi(X,t)}{\epsilon}} \sum_{n} \mathbf{a}_{n}(X,t)\epsilon^{n}, \tag{6.1a}$$

$$p'(X,t) = e^{i\frac{\phi(X,t)}{\epsilon}} b(X,t,\epsilon) = e^{i\frac{\phi(X,t)}{\epsilon}} \sum_{n} b_n(X,t)\epsilon^{n+1}, \tag{6.1b}$$

where  $\phi$  denotes the eikonal function, whose spatial derivatives represent the local wavenumber components  $k = \nabla \phi(X, t)$ , while  $\epsilon \ll 1$  is a small parameter expressing the smallness of the scale of the waves represented by (6.1).

Substituting the expansions (6.1a)–(6.1b) into the perturbation equations (3.4) and grouping terms multiplied by the same power of  $\epsilon$ , a hierarchy of equations is obtained. The leading-order approximation yields a set of ordinary differential equations (ODEs) that, in the inviscid  $(Re \to \infty)$  and short-wave  $(||k|| \to \infty)$  limits, provide the growth rate associated with a localised perturbation. Specifically, the system of equations describes the evolution of the wavenumber vector k and the amplitude a as follows:

$$\begin{cases} \frac{D\mathbf{k}}{\mathrm{D}t} = -\mathcal{L}^{T}(\mathbf{X})\mathbf{k}, \\ \frac{D\mathbf{a}}{\mathrm{D}t} = \left(\frac{2\mathbf{k}\mathbf{k}^{T}}{|\mathbf{k}|^{2}} - \mathcal{I}\right)\mathcal{L}(\mathbf{X})\mathbf{a}, \end{cases}$$
(6.2)

where X is the position of the fluid particle moving along the streamlines of the steady base flow

$$\frac{\mathrm{D}X(t)}{\mathrm{D}t} = \mathbf{u}_b(X(t), t). \tag{6.3}$$

In the above equations, D/Dt represents the so-called material derivative (i.e.  $D/Dt = \partial/\partial t + u_b \cdot \nabla$ ),  $\mathcal{L} = \nabla u_b$  denotes the base-flow velocity-gradient tensor,  $\mathcal{L}$  is the identity matrix and the superscript T denotes the transpose. Lifschitz & Hameiri (1991) proved that the flow is unstable if there exists a streamline along which the amplitude a(t) grows without bound as  $t \to \infty$ . Since the inviscid structural sensitivity analysis (§ 5) suggested the occurrence of an elliptic amplification process, we evaluated the inviscid local stability equations (6.2) at the vortex centre of the primary recirculation bubble (thereby, following the work of Bayly 1986, the tensor  $\mathcal{L}$  has been computed at this point).

Provided k(t) is periodic in time, the second equation of (6.2) is a Floquet problem for a(t). As is well known (Bender & Orszag 2013), the general solution is a linear superposition of Floquet modes

$$\boldsymbol{a}(t) = \bar{\boldsymbol{a}}(t)e^{\gamma t},\tag{6.4}$$

where  $\bar{a}(t)$  is a periodic function with the same period  $(T_p)$  as k, while  $\gamma$  is the corresponding complex Floquet exponent, to be determined by computing the monodromy matrix  $\mathscr{A}(T_p)$  that satisfies

$$\frac{\mathcal{D}\mathscr{A}}{Dt} = \left(\frac{2kk^T}{|k^2|} - \mathscr{I}\right) \mathscr{L}(X)\mathscr{A} \quad \text{with } \mathscr{A}(0) = \mathscr{I}. \tag{6.5}$$

Thus, the instability problem reduces to the calculation of the matrix  $\mathscr{A}$  and its non-trivial eigenvalues ( $\gamma_i$  with i=1,2,3). Assuming that the real parts ( $\mu_i$ ) of such eigenvalues satisfy the condition  $\mu_1 > \mu_2 > \mu_3$ , the asymptotic growth rate is given by the simple relation

	LSA			WKB	Error
$\sigma_A(k_A = 1.77)$	$\sigma_B(k_B = 2.08)$	ξ	$\sigma_0(k\to\infty)$	$\sigma_{\infty}$	(%)
0.05166	0.05922	0.0898	0.1024	0.09143	10.71

Table 1. Comparison between the amplification rates given by the LSA and that given by the short-wave asymptotics (WKB) in the centre of the primary recirculation bubble ( $\sigma_{\infty}$ ). The last column estimates the discrepancy between the two methods.  $\xi$  and  $\sigma_0$  are extrapolated from the results shown in the plane  $(k, \sigma)$  (see figure 8a in § 5) using the points  $A = (k_A, \sigma_A) = (1.77, 0.05166)$  and  $B = (k_B, \sigma_B) = (2.08, 0.05922)$  and assuming a relation of the form  $\sigma = \sigma_0 - \xi/k$  (from Sipp et al. 1999).

$$\sigma_{\infty} = \frac{\log(\mu_1)}{T_n},\tag{6.6}$$

where  $T_p$  denotes the period of revolution of k

To validate our numerical implementation of the asymptotic approach, we replicated Bayly's analytical results (Bayly 1986) (as detailed in Appendix B) and subsequently used this numerical tool to compute the amplification rate  $(\sigma_{\infty})$  for the problem under investigation.

#### 6.2. Results

The asymptotic amplification rate  $(\sigma_{\infty})$ , computed in the centre of the primary vortex, is displayed in the fifth column of table 1. To make a quantitative comparison between the results obtained from the local and global stability analysis, we followed the work of Sipp *et al.* (1999). Therefore, considering a relation of the type

$$\sigma(k) = \sigma_0 - \frac{\xi}{k},\tag{6.7}$$

we computed an extrapolated value of the (global) growth rate in the limit of large wavenumbers, namely  $\sigma(k \to \infty) = \sigma_0$ . In particular, the parameters of (6.7), i.e.  $\sigma_0$  and  $\xi$  (the latter called the eigenvalue convergence parameter), have been evaluated using the amplification rates  $(\sigma_A, \sigma_B)$  and the corresponding wavenumbers  $(k_A, k_B)$  given by the global LSA, for the last two cases investigated using the inviscid sensitivity protocol (indicated in figure 8a of § 5 with A and B, while in table 1 they are denoted  $\sigma_A$  and  $\sigma_B$ ).

As reported in the sixth column of table 1, the discrepancy in percentage between the predictions provided by the two theories (global,  $\sigma_0$  and local,  $\sigma_\infty$ ) is approximately 10 %.

Figure 10a shows the comparison between the global growth rates and those predicted through (6.7). A good agreement is observed between the two sets of data. In particular, the global stability analysis is more computationally expensive with respect to the geometric optics approach, since the computation of a global eigenpair involves the solution of a two-dimensional generalised EVP, while the WKB approach involves the simple integration of a tiny set of ODEs in one dimension.

Figure 10b shows how the global least stable spanwise wavenumber k grows with the Reynolds number ( $Re_{STB}$ ). In particular, it increases almost linearly with the logarithm of  $Re_{STB}$ . This is in agreement with the hypothesis of the asymptotic theory, suggesting that k will tend to infinity in the limit of vanishing viscosity.

## 7. Discussion and conclusions

This paper investigates the inviscid mechanism, driving the secondary instability in a 1:3 planar sudden expansion, through a sensitivity-based approach. The key ingredient of this

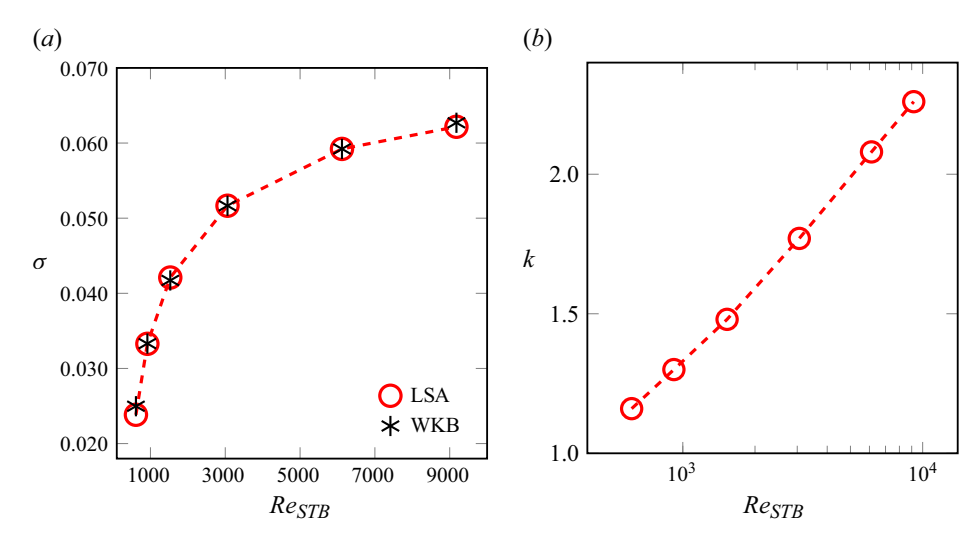


Figure 10. (a) Comparison between the maximum amplification rates  $\sigma$  (i.e. the y coordinate of the red markers of figure 8a) given by the LSA (lines) and those predicted by the WKB method using the relation proposed by Sipp et al. (1999). (b) Spanwise wavenumber k at maximum growth rate (i.e. the abscissa of the red markers of figure 8a) as a function of  $Re_{STB}$ . A logarithmic scale is used on the x-axis only for panel (b).

methodology lies in making viscosity effects vanish solely in the global stability equations, while maintaining the base-flow field constant, computed at the critical Reynolds number. This is practically implemented by decoupling the Reynolds number that serves as the control parameter for determining the steady base flow  $(Re_{BF})$  from that governing the disturbance evolution  $(Re_{STB})$ . A structural sensitivity analysis is subsequently performed, with  $Re_{STB}$  progressively increased in the linearised equations. The resulting inviscid structural sensitivity map  $(S^*)$  reveals the flow regions where the instability mechanism acts.

The analysis is first carried out by means of the global LSA to accurately estimate the instability threshold (§ 3). Specifically, the numerical results indicate that the base flow undergoes a steady, three-dimensional bifurcation at a critical Reynolds number of approximately  $Re_{cr}^{(II)} \approx 306$ , associated with a spanwise wavenumber  $k \approx 0.65$ . Subsequently, the spatial structure of the direct and adjoint eigenmodes is examined to characterise the flow features beyond the bifurcation point. The overlap of these two fields (§ 4) provides information about the sensitivity properties of the flow, the so-called wavemaker region, where the amplification of the perturbations and receptivity combine to trigger the instability. In particular, the primary recirculation bubble emerges as the most sensitive region, as the norm of the structural sensitivity tensor (S) is concentrated therein, with its peak spread near the primary vortex centre.

The relatively compact spatial support of the sensitivity map suggests that the instability may be associated with an inviscid amplification process. To test this hypothesis and clarify the underlying physical mechanism, the inviscid structural sensitivity analysis proves to be an indispensable tool (§ 5). This approach clearly identifies the core of the instability with the vortex centre of the primary recirculation region, thereby assessing the elliptical nature of the instability.

In summary, our findings indicate that the classical structural sensitivity (S) effectively identifies the wavemaker within the primary recirculation bubble (see figure 6 of § 4). However, it is only the inviscid structural sensitivity field (S\*) that reveals that the

instability core is concentrated in the centre of an elliptical vortex (see figure 8d). We stress here that the structure of the sensitivity field observed in the original analysis is affected by viscous effects, which spread and shift the core of the instability. While the classical structural sensitivity is capable of locating the region where the instability mechanism is acting, when the mechanism is inviscid the presence of viscosity blurs the picture, preventing a precise assessment of the active mechanism. To remove this ambiguity, one has to isolate the inviscid effects to shed light on the instability mechanism. In this respect, the inviscid structural sensitivity helps to clarify the picture, and it allowed us to clearly identify the instability mechanism by highlighting the vortex core as responsible for the instability.

Referring to the energetic approach developed by Lanzerstorfer & Kuhlmann (2012a), both methods lead to the same conclusion for large expansion ratios, where the instability is oscillatory (as discussed in 5.3). However, for moderate expansion ratios, such as the 1:3 sudden expansion case (which is the focus of the present study, characterised by a stationary critical mode), the energetic approach does not provide evidence of an inviscid mechanism. Indeed, the authors attributed the physical nature of the instability to a combination of streamline convergence, shear stress and deceleration, as all the integral production rates were found to be positive, thus preventing them from assessing the inviscid mechanism and its specific location. Through the inviscid structural sensitivity analysis, we demonstrate that an elliptic instability is already present in the steady regime (i.e. for moderate expansion ratios), thereby completing the picture provided by Lanzerstorfer & Kuhlmann.

Subsequently (in § 6), the geometric optics technique is introduced to validate the predictions given by the global approach. In particular, the amplification rate, evaluated in the centre of the primary vortex by the local theory, is in complete agreement with that obtained from the sensitivity protocol, confirming the inviscid character of the instability. Thereby, we precisely identify, through both methods, an elliptic mode instability. To the best of our knowledge this is the first time that inviscid structural sensitivity analysis has been successfully employed to detect an elliptic type instability, in agreement with predictions from geometric optics.

In conclusion, inviscid structural sensitivity analysis, discussed in this paper, is a general concept that can be applied whenever the instability in question is of an inviscid nature. The flow in a plane symmetric sudden expansion represents a prototype of geometrical configurations characterised by a finite region of separated flow. Therefore, a natural question arises regarding how the breakdown of these eddies would occur, influencing the overall behaviour of the system. Identifying the operating instability mechanism and determining whether it is viscous or inviscid is important because different instability mechanisms involve distinct behaviours of the flow dynamics. Inviscid instability mechanisms underlie many important phenomena (Pierrehumbert 1986), such as the vortex breakdown: 'a universal mechanism whereby complex three-dimensional motion can arise directly from large-scale two-dimensional coherent structures' (Bayly 1986).

**Funding.** We acknowledge financial support under the National Recovery and Resilience Plan (PNRR), Mission 4, Component 2, Investment 1.1, Call for tender No. 1409 published on 14.9.2022 by the Italian Ministry of University and Research (MUR), funded by the European Union - NextGenerationEU - Project Title: IMPULJET - CUP D53D23018400001 - Grant Assignment Decree No. 1385 adopted on 01/09/2023 by the Italian Ministry of University and Research (MUR).

**Declaration of interests.** The authors report no conflict of interest.

# Appendix A. Numerical method for the global analysis

The numerical methodology is the same as that of Citro *et al.* (2015), where details and references can be found. The open-source FreeFEM++ software (Hecht 2012), based on a finite element method, has been used to solve both the base-flow problem and the stability EVP.

# A.1. Base flow

The Navier–Stokes equations, written in weak formulation, are discretised by projecting the flow field upon a basis of Taylor–Hood finite elements, using quadratic elements (P2) for the velocity and linear elements (P1) for the pressure.

The base flow is obtained by solving the two-dimensional, steady version of the Navier–Stokes equations, (3.3), along with the boundary conditions, using the standard Newton–Raphson procedure: given an initial guess  $\boldsymbol{w}_{b}^{(0)}$ , the linear system

$$NS\left(Re_{BF}, \boldsymbol{W}_{b}^{(n)}\right) \cdot \boldsymbol{w}_{b}^{(n)} = -rhs^{(n)}, \tag{A1}$$

is solved at each iteration step using the multifrontal massively parallel sparse solver (Amestoy *et al.* 2001, 2006) for the matrix inversion. In particular,  $W_b^{(n)}$  denotes the base flow at the *n*th iteration, while *rhs* indicates the right-hand side of the governing equations.

The base flow is then updated as

$$\mathbf{W}_{b}^{(n+1)} = \mathbf{W}_{b}^{(n)} + \mathbf{w}_{b}^{(n)}. \tag{A2}$$

The initial guess is chosen to be the solution of the Stokes equations and the process is continued until the  $L^2$ -norm of the residual of the governing equations becomes smaller than a given tolerance.

# A.2. Eigenvalue solver

Once the base flow is obtained, the EVP (3.7) is used to perform the stability analysis.

The governing equations (3.7) and their boundary conditions can be recasted into the algebraic generalised EVP

$$[A(Re_{STB}, W_b(Re_{BF})) + \gamma B] \cdot w = 0, \tag{A3}$$

where w is the right (or direct) eigenvector and A, B are the two matrices obtained from the spatial discretization of the differential operators. The system (A3) is solved using the implicitly restarted Arnoldi method (Arnoldi 1951) implemented in the ARPACK library (Lehoucq, Sorensen & Yang 1998) in FreeFem++.

The solution of the linear systems in the Arnoldi iterations is obtained by the same sparse solver (Amestoy *et al.* 2001, 2006) used for the base-flow calculations. The adjoint eigenmodes, necessary to evaluate the sensitivity tensor and to inspect the receptivity of the mode, have been computed as the left eigenvectors of the discretised system. Then, the sensitivity function is computed by the product of the direct and adjoint fields. In particular, the right (direct) and left (adjoint) eigenvectors are normalised by requiring

$$\max_{x,y \in \mathcal{D}} \{|\hat{\boldsymbol{u}}(x,y)|\} = 1, \qquad \int_{\mathcal{D}} \hat{\boldsymbol{u}}^{\dagger} \cdot \hat{\boldsymbol{u}} = 1.$$
 (A4)

# Appendix B. Validation of the local solver

The asymptotic inviscid stability analysis (§ 5) relies on the same steady base flow used for the global stability computations. The system of ODEs (6.2) is solved using a

classical fourth-order, Runge–Kutta scheme, starting from the initial conditions. Then, the fundamental Floquet matrix  $\mathscr{A}$  is evaluated.

In the present section, we provide a validation test to assess the effectiveness of this numerical tool, by reproducing the analytical results of Bayly (1986) that, inspired by Pierrehumbert's findings (Pierrehumbert 1986) on elliptical instability, proposed a simple mathematical model to shed light on the feedback mechanism involved.

He examined the stability of a two-dimensional inviscid flow, described by the following velocity field:

$$\boldsymbol{u}(x, y, z) = \Omega\left(-Ey, \frac{1}{E}x, 0\right), \text{ with } \Omega > 0, E > 1,$$
 (B1)

which approximates the flow near an elliptical stagnation point in the x-y plane.

The streamlines of (B1) constitute a family of similar ellipses, with the major (x) and minor (y) axes in the ratio E, that represents a measure of the eccentricity of the elliptical streamlines. In particular, if E = 1, the flow given by (B1) becomes a state of rigid rotation about the z-axis at a rate of  $\Omega$ . While E > 1 indicates the elliptic case.

Recalling the system of (6.2), presented in § 6 and reproduced here for convenience

$$\frac{D\mathbf{k}}{Dt} = -\mathcal{L}^T \mathbf{k},\tag{B2a}$$

$$\frac{D\mathbf{a}}{Dt} = \left(\frac{2\mathbf{k}\mathbf{k}^T}{|\mathbf{k}|^2} - \mathscr{I}\right) \mathscr{L}\mathbf{a},\tag{B2b}$$

the general solution of (B2a) is

$$\mathbf{k}(t) = k_0 \left( \sin \theta \cos \left( \Omega(t - t_0) \right), E \sin \theta \sin \left( \Omega(t - t_0) \right), \cos \theta \right), \tag{B3}$$

which describes the motion on an ellipse parallel to the x-y plane.

In particular,  $k_0$  is a measure of the magnitude of the wave vector and  $t_0$  is the delay time, i.e. an arbitrary quantity that serves only to specify the phase angle of the rotation. The wave vector  $\mathbf{k}$  precesses elliptically with a circular frequency  $\Omega$  and (minimum) inclination angle  $\theta$  with respect to the z-axis.

Since k(t) is periodic in time, (B2b) is a Floquet problem for a(t). Thus, the instability problem reduces to the calculation of the monodromy matrix  $\mathscr A$  and its non-trivial eigenvalues, that depend only on the eccentricity E and the inclination angle  $\theta$ . Given E, we are particularly interested in the maximum value of the growth rate  $(\sigma)$  and the angle  $(\theta_{max})$  at which it is attained. Following Bayly, we have computed the eigenvalues of the fundamental Floquet matrix  $(\mathscr A)$  for any reasonable values of E > 1 and  $0 < \theta < \pi/2$ . The comparison between our results and those obtained by Bayly is illustrated in the plane  $(E,\theta)$  of figure 11. The three curves (indicated with letters a,b and c) are the results obtained by Bayly. In particular, the dashed (a), solid (b) and dotted (c) curves indicate, respectively, the largest angle giving the instability  $\theta_+(E)$ , the angle at which the growth rate is maximised  $\theta_{max}(E)$  and the smallest angle giving instability  $\theta_-(E)$ . Curves a and c are the so-called 'neutral' curves, since they separate the stable (S) and unstable (I) regions in the plane  $(E,\theta)$ .

The contour plot shows our findings, i.e. the maximum value of the asymptotic growth rate  $\sigma$ , for each eccentricity E and angle  $\theta$ . It is evident that for any E > 1, there is a band of angles  $\theta$  for which there is a real positive Floquet exponent  $\sigma$ . This interval shrinks down to the point  $\theta = \pi/3$  as  $E \to 1$  and remains bounded away from both  $\theta = 0$  and

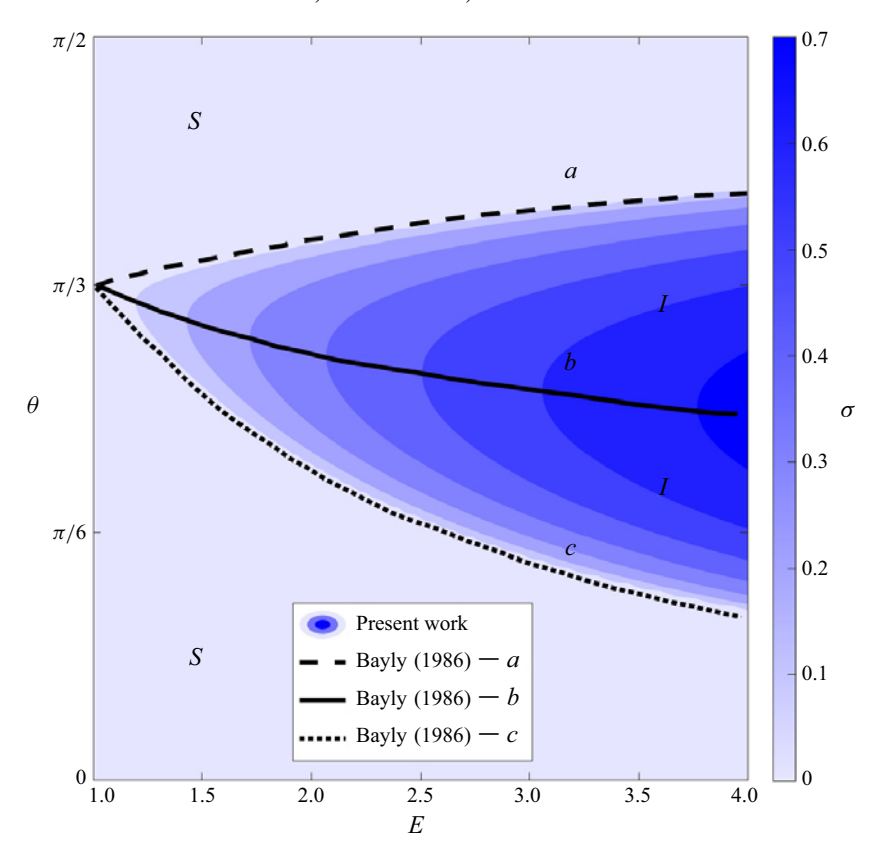


Figure 11. Validation of the numerical implementation used for the asymptotic analysis: the three curves indicate the analytical outcomes of Bayly (1986), while the contour plot displays our numerical results.

 $\theta = \pi/2$  for all 1 < E < 4. Our results lie very closely to Bayly's curves, confirming the correctness of our numerical implementation.

#### REFERENCES

AMESTOY, P.R., DUFF, I.S., L'EXCELLENT, J.-Y. & KOSTER, J. 2001 A fully asynchronous multifrontal solver using distributed dynamic scheduling. SIAM J. Matrix Anal. A. 23 (1), 15–41.

AMESTOY, P.R., GUERMOUCHE, A., L'EXCELLENTJ.-Y. & PRALETS. 2006 Hybrid scheduling for the parallel solution of linear systems. *Parallel Comput.* 32 (2), 136–156.

ARNOLDI, W.E. 1951 The principle of minimized iterations in the solution of the matrix eigenvalue problem. *Q. Appl. Math.* **9** (1), 17–29.

BATTAGLIA, F., TAVENER, S.J., KULKARNI, A.K. & MERKLE, C. L. 1997 Bifurcation of low Reynolds number flows in symmetric channels. *AIAA J.* 35 (1), 99–105.

BAYLY, B.J. 1986 Three-dimensional instability of elliptical flow. Phys. Rev. Lett. 57 (17), 2160.

BAYLY, B.J. 1988 Three-dimensional centrifugal-type instabilities in inviscid two-dimensional flows. *Phys. Fluids* 31 (1), 56–64.

BAYLY, B.J. 1989 Computations of broad-band instabilities in a class of closed-streamline flows. In *Mathematical aspects of vortex dynamics; Proceedings of the Workshop, Leesburg, VA*, pp. 50–58.

BENDER, C.M. & ORSZAG, S.A. 2013 Advanced Mathematical Methods for Scientists and Engineers: Asymptotic Methods and Perturbation Theory, vol. 1. Springer Science & Business Media.

BOURQUE, C. & NEWMAN, B.G. 1960 Reattachment of a two-dimensional, incompressible jet to an adjacent flat plate. *Aeronaut. Quart.* 11 (3), 201–232.

CHARRU, F. 2011 Hydrodynamic Instabilities, vol. 37. Cambridge University Press.

CHERDRON, W., DURST, F. & WHITELAW, J.H. 1978 Asymmetric flows and instabilities in symmetric ducts with sudden expansions. *J. Fluid Mech.* **84** (1), 13–31.

- CHIARINI, A. & AUTERI, F. 2023 Linear global and asymptotic stability analysis of the flow past rectangular cylinders moving along a wall. *J. Fluid Mech.* **966**, A22.
- CITRO, V., GIANNETTI, F., BRANDT, L. & LUCHINI, P. 2015 Linear three-dimensional global and asymptotic stability analysis of incompressible open cavity flow. J. Fluid Mech. 768, 113–140.
- DURST, F., MELLING, A. & WHITELAW, J.H. 1974 Low Reynolds number flow over a plane symmetric sudden expansion. *J. Fluid Mech.* **64** (1), 111–128.
- DURST, F., PEREIRA, J.C.F. & TROPEA, C. 1993 The plane symmetric sudden-expansion flow at low Reynolds numbers. *J. Fluid Mech.* **248**, 567–581.
- FANI, A., CAMARRI, S. & SALVETTI, M.V. 2012 Stability analysis and control of the flow in a symmetric channel with a sudden expansion. *Phys. Fluids* **24** (8), 084102.
- FEARN, R.M., MULLIN, T. & CLIFFE, K.A. 1990 Nonlinear flow phenomena in a symmetric sudden expansion. *J. Fluid Mech.* 211, 595–608.
- FIEDLER, H.E. 1987 Coherent structures. In Advances in Turbulence: Proceedings of the First European Turbulence Conference Lyon, France, 1–4 July 1986, Springer, pp. 320–336.
- FRIEDLANDER, S. & VISHIK, M.M. 1991 Instability criteria for the flow of an inviscid incompressible fluid. *Phys. Rev. Lett.* **66** (17), 2204.
- GALLAIRE, F., MARQUILLIE, M. & EHRENSTEIN, U. 2007 Three-dimensional transverse instabilities in detached boundary layers. *J. Fluid Mech.* **571**, 221–233.
- GIANNETTI, F. & LUCHINI, P. 2007 Structural sensitivity of the first instability of the cylinder wake. *J. Fluid Mech.* **581**, 167–197.
- GODEFERD, F.S., CAMBON, C. & LEBLANC, S. 2001 Zonal approach to centrifugal, elliptic and hyperbolic instabilities in stuart vortices with external rotation. *J. Fluid Mech.* 449, 1–37.
- HAWA, T. & RUSAK, Z. 2000 Viscous flow in a slightly asymmetric channel with a sudden expansion. *Phys. Fluids* 12 (9), 2257–2267.
- HECHT, F. 2012 New development in freefem++. J. Numer. Math. 20, 251-266.
- HUERRE, P. & MONKEWITZ, P.A. 1990 Local and global instabilities in spatially developing flows. Annu. Rev. Fluid Mech. 22 (1), 473–537.
- KERSWELL, R.R. 2002 Elliptical instability. Annu. Rev. Fluid Mech. 34 (1), 83-113.
- LANDMAN, M.J. & SAFFMAN, P.G. 1987 The three-dimensional instability of strained vortices in a viscous fluid. Phys. Fluids 30 (8), 2339–2342.
- LANZERSTORFER, D. & KUHLMANN, H.C. 2012a Global stability of multiple solutions in plane suddenexpansion flow. *J. Fluid Mech.* **702**, 378–402.
- LANZERSTORFER, D. & KUHLMANN, H.C. 2012b Global stability of the two-dimensional flow over a backward-facing step. J. Fluid Mech. 693, 1–27.
- LANZERSTORFER, D. & KUHLMANN, H.C. 2012c Three-dimensional instability of the flow over a forward-facing step. J. Fluid Mech. 695, 390–404.
- LEBLANC, S. 1997 Stability of stagnation points in rotating flows. Phys. Fluids 9 (11), 3566–3569.
- LEBLANC, S. & CAMBON, C. 1997 On the three-dimensional instabilities of plane flows subjected to coriolis force. *Phys. Fluids* **9** (5), 1307–1316.
- LEBOVITZ, N.R. & LIFSCHITZ, A. 1996 Short-wavelength instabilities of riemann ellipsoids. *Phil. Trans. Royal Soc. London. Series A: Math. Phys. Engine. Sci.* **354** (1709), 927–950.
- LEHOUCQ, R.B., SORENSEN, D.C. & YANG, C. 1998 ARPACK Users' Guide: Solution of Large-Scale Eigenvalue Problems with Implicitly Restarted Arnoldi Methods. Society for Industrial and Applied Mathematics (SIAM).
- Leweke, T. & Williamson, C.H.K. 1998 Cooperative elliptic instability of a vortex pair. *J. Fluid Mech.* **360**, 85–119.
- LIFSCHITZ, A. 1994 On the instability of certain motions of an ideal incompressible fluid. *Adv. Appl. Math.* **15** (4), 404–436.
- LIFSCHITZ, A. & HAMEIRI, E. 1991 Local stability conditions in fluid dynamics. *Phys. Fluids A: Fluid Dyn.* **3** (11), 2644–2651.
- LUCHINI, P. & BOTTARO, A. 2014 Adjoint equations in stability analysis. *Annu. Rev. Fluid Mech.* 46 (1), 493–517.
- PIERREHUMBERT, R.T. 1986 Universal short-wave instability of two-dimensional eddies in an inviscid fluid. *Phys. Rev. Lett.* **57** (17), 2157.
- PRALITS, J.O., GIANNETTI, F. & BRANDT, L. 2013 Three-dimensional instability of the flow around a rotating circular cylinder. *J. Fluid Mech.* **730**, 5–18.
- QADRI, U.A., CHANDLER, G.J. & JUNIPER, M.P. 2015 Self-sustained hydrodynamic oscillations in lifted jet diffusion flames: origin and control. J. Fluid Mech. 775, 201–222.

- QADRI, U.A., MISTRY, D. & JUNIPER, M.P. 2013 Structural sensitivity of spiral vortex breakdown. J. Fluid Mech. 720, 558–581.
- RAYLEIGH, L. 1879 On the stability, or instability, of certain fluid motions. *Proc. London Mathe. Soc. s1*-11(1), 57–72.
- RAYLEIGH, L. 1917 On the dynamics of revolving fluids. *Proc. Royal Soc. London. Series A, Containing Papers Mathe. Phys. Charact.* **93** (648), 148–154.
- SIPP, D. & JACQUIN, L. 1998 Elliptic instability in two-dimensional flattened Taylor-green vortices. *Phys. Fluids* 10 (4), 839–849.
- SIPP, D., LAUGA, E. & JACQUIN, L. 1999 Vortices in rotating systems: centrifugal, elliptic and hyperbolic type instabilities. *Phys. Fluids* **11** (12), 3716–3728.
- SOBEY, I.J. & DRAZIN, P.G. 1986 Bifurcations of two-dimensional channel flows. J. Fluid Mech. 171, 263-287.
- THEOFILIS, V. 2011 Global linear instability. Annu. Rev. Fluid Mech. 43 (1), 319-352.
- WALEFFE, F. 1990 On the three-dimensional instability of strained vortices. *Phys. Fluids A: Fluid Dyn.* 2 (1), 76–80.